Soil Salinity Impacts on L-Band Remote Sensing of Soil Moisture

Kaighin A. McColl, *Member, IEEE*, Dongryeol Ryu, *Member, IEEE*, Vjekoslav Matic, Jeffrey P. Walker, Justin Costelloe, and Christoph Rüdiger

***Abstract*—The recently launched Soil Moisture and Ocean Salinity (SMOS) satellite is providing soil moisture observations at continental scales by measuring L-band microwave radiation emitted from the land surface. While its retrieval algorithms will correct for factors such as vegetation and surface roughness, it will not correct for soil salinity. This letter tests the assumption that soil salinity will have a negligible impact on L-band brightness temperature (T_b) at SMOS scales using field data; airborne T_b observations were collected in a saline groundwater discharge area near Nilpinna Station, South Australia. At the 500-m scale, the airborne observations of T_b could not be reproduced using the baseline algorithm of the SMOS Level 2 retrieval scheme, without accounting for soil salinity in the model. The analysis in this letter shows that soil moisture retrieval errors of at least 0.04 m^3m^{-3} (i.e., the entire SMOS error budget) will occur due to salinity alone in SMOS footprints with saline coverage as low as 25% (possibly even much less). Consequently, fractional salinity coverage cannot be considered a negligible factor by microwave soil moisture satellite missions.**

***Index Terms*—Microwave radiometry, soil moisture, Soil Moisture and Ocean Salinity (SMOS), soil salinity.**

I. Introduction

PASSIVE microwave soil moisture missions at L-band (~1.4 GHz) show significant promise in measuring soil moisture at global and continental scales, due to their relative sensitivity to soil moisture, insensitivity to vegetation, and independence of weather conditions [1]. The Soil Moisture and Ocean Salinity (SMOS) mission, launched in November 2009, is providing soil moisture estimates from L-band radiation emitted from the Earth's surface using an interferometric radiometer [2]. Significant effort has been made to correct for effects on the signal due to vegetation, surface roughness, and soil properties (e.g., [3] and [4]). However, to date, there have been no attempts to correct the effects of salinity on satellite or airborne data, despite existing laboratory experiments [5], [6] and model simulations [7] showing that soil salinity may have a large effect on the microwave signal. While past field studies have either been inconclusive [5]–[8] or found the soil salinity effects to be small [9], none were conducted in naturally saline areas, where salinity effects can be pronounced. With approximately 7% of the Earth's continental surface area highly salt affected [10], failing to account for soil salinity effects could compromise soil moisture satellite missions. Consequently, this letter investigates the effects of soil salinity on L-band microwave emissions in a saline environment, using airborne L-band and thermal infrared (TIR) observations.

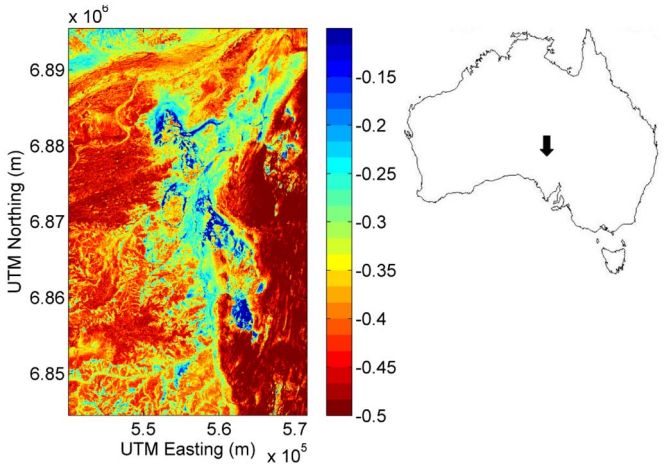

Fig. 1. Study site at Nilpinna Station (31.5 km × 51 km). The background image shows Landsat-derived NDWI (−), highlighting (dark blue) groundwater discharge areas. Coordinates are for Zone 53J UTM. The NDWI image was taken on October 20, 2008.

II. Data

The data for this study were collected in the arid region around Nilpinna Station, South Australia (lower left corner: 540 140 mE, 6 844 477 mN of Universal Transverse Mercator (UTM) Zone 53J; upper right corner: 571 640 mE, 6 895 477 mN of UTM Zone 53J; see Fig. 1), as part of an airborne field experiment. Despite low annual rainfall (approximately 173 mm/year), groundwater discharge through the soil surface from an underlying confined aquifer leads to regions of very high soil moisture. Evapo-concentration of the moderately saline groundwater in the near-surface environment results in high soil salinity. However, despite the moist conditions, no standing water was observed at the site. Note that, in Fig. 1, the highest normalized difference wetness index (NDWI) observed at the site was −0.10; NDWI is normally positive for open water [11], indicating that no standing water was present. While 23 mm of rain fell in the three weeks between the satellite overpass and the field experiment, any standing water would

Manuscript received January 21, 2011; revised May 17, 2011 and July 10, 2011; accepted August 3, 2011. Date of publication October 6, 2011; date of current version February 8, 2012. This work was supported in part by the Australian Research Council under Grant DP0879212.

K. A. McColl, D. Ryu, V. Matic, and J. Costelloe are with the Department of Infrastructure Engineering, The University of Melbourne, Melbourne, Vic. 3010, Australia (e-mail: kmccoll@unimelb.edu.au; dryu@unimelb.edu.au; v.matic@pgrad.unimelb.edu.au; jcost@unimelb.edu.au).

J. P. Walker and C. Rüdiger were with the Department of Infrastructure Engineering, The University of Melbourne, Melbourne, Vic. 3010, Australia. They are now with the Department of Civil Engineering, Monash University, Clayton, Vic. 3800, Australia (e-mail: jeff.walker@monash.edu; chris.rudiger@monash.edu).

Digital Object Identifier 10.1109/LGRS.2011.2165932

have all evaporated by the start of the field experiment due to the high potential evapotranspiration at Nilpinna (an average of 165 mm for the month of November). Thus, the NDWI image is representative of the steady-state conditions at Nilpinna during the field experiment, with no standing water present. There is very little vegetation at the site.

On November 12, 2008, L-band brightness temperature (T_b) was measured using the Polarimetric L-band Multibeam Radiometer (PLMR) mounted on board an experimental aircraft (at a flight altitude of 1500 m above ground level). The radiometer measured horizontally and vertically polarized radiations at six viewing angles ($\pm 7^\circ, \pm 21.5^\circ$, and $\pm 38.5^\circ$), but only the horizontally polarized measurements (T_{bh}) were considered reliable for this study. Broadband TIR radiometers were also installed at the same incidence angles to provide coincident footprints with those of the PLMR. Both L-band and TIR measurements were mapped to 500-m grids over the majority of the groundwater discharge area (i.e., the eastern part of the map in Fig. 1) and 1000-m grids over the remaining areas.

III. Soil Moisture Retrieval

The single-channel $\tau-\omega$ radiative transfer model is used in this work, since it is a baseline model adopted by SMOS [14]. For nonvegetated surfaces such as those at Nilpinna, T_{bh} is related to the soil emissivity by

$$T_{bh} = eT_e \tag{1}$$

where e is the horizontally polarized emissivity of the land surface and T_e is the effective temperature of the soil surface. In this study, T_e is approximated by the airborne TIR observations. Sensitivity tests showed that the results of this letter are robust to reasonable changes in T_e, demonstrating that the approximation is valid for this study. The surface emissivity can be derived by (e.g., [15] and [16])

$$e = 1 - \Gamma \exp(h) \tag{2}$$

where Γ is the surface reflectivity (assumed to approximate the soil reflectivity) and h varies with soil moisture as given by [16]

$$h = \begin{cases} h_0 - 4.4(\theta - \theta_{\text{fc}}), \theta \leq \theta_{\text{fc}} \\ h_0, \theta > \theta_{\text{fc}} \end{cases} \tag{3}$$

where h_0 is taken to be 0.10, a representative value for desert/tundra [15], and θ_{fc} is the field capacity, set to 0.21 m^3m^{-3} in this work, a typical value for sandy loam [17]. The results of this study are robust to reasonable changes in h. The Fresnel equations and Dobson dielectric model [18] are used to calculate soil moisture. In addition to the default $\tau-\omega$ model equations described previously, a soil salinity model is applied in saline soil moisture cases [19]. Three variables in the Dobson model are dependent on salinity: the effective conductivity σ_i, relaxation time τ_w, and static dielectric constant of water ε_{w0}. For pure water (with $\sigma_i = 0$), they are given by

$$2\pi\tau_w(T) = 1.1109 \times 10^{-10} - 3.824 \times 10^{-12}T + 6.938 \times 10^{-14}T^2 - 5.096 \times 10^{-16}T^3 \tag{4}$$

$$\varepsilon_{w0}(T) = 88.045 - 0.4147T + 6.2958 \times 10^{-4}T^2 + 1.075 \times 10^{-5}T^3. \tag{5}$$

The salinity model considers water with salinity less than 4000 ppm to be "pure." Water with salinity in the range of 4000–35 000 ppm (i.e., up to approximately the same salinity as seawater) is classified "saline." The effective conductivity σ_i (in siemens per meter) for water in this range is given by [7], [20]

$$\sigma_i = S_{SW}\left(0.18252 - 1.4619 \times 10^{-3}S_{SW} + 2.093 \times 10^{-5}S_{SW}^2 - 1.282 \times 10^{-7}S_{SW}^3\right) e^{-\phi}$$

where

$$\phi = \Delta\left(2.033 \times 10^{-2} + 1.266 \times 10^{-4}\Delta + 2.464 \times 10^{-6}\Delta^2 - S_{SW}(1.849 \times 10^{-5} - 2.551 \times 10^{-7}\Delta + 2.551 \times 10^{-8}\Delta^2)\right) \tag{7}$$

$$\Delta = 25 - T. \tag{8}$$

The relaxation time τ_{SW} for "saline" water is then given by

$$\tau_{sw} = \tau_w\left(1.0 + 2.282 \times 10^{-5}TS_{sw} - 7.638 \times 10^{-4}S_{sw} - 7.760 \times 10^{-6}S_{sw}^2 + 1.105 \times 10^{-8}S_{sw}^3\right). \tag{9}$$

The static dielectric constant of "saline" water ε_{SW0} is given by

$$\varepsilon_{sw0} = (87.134 - 1.949 \times 10^{-1}T - 1.276 \times 10^{-2}T^2 + 2.491 \times 10^{-4}T^3) \times \left(1.0 + 1.613 \times 10^{-5}TS_{sw} - 3.656 \times 10^{-3}S_{sw} + 3.210 \times 10^{-5}S_{sw}^2 - 4.232 \times 10^{-7}S_{sw}^3\right). \tag{10}$$

Water with high salt concentrations (i.e., with salinity greater than 35 000 ppm) is classified "brine." In this case, we have

$$\sigma_i = N_b\left(10.39 - 2.378N_b + 0.683N_b^2 - 0.135N_b^3 + 1.01 \times 10^{-2}N_b^4\right) \times \left(1.0 - 1.96 \times 10^{-2}\Delta + 8.08 \times 10^{-5}\Delta^2 - N_b\Delta(3.02 \times 10^{-5} + 3.92 \times 10^{-5}\Delta + N_b\left(1.72 \times 10^{-5} - 6.58 \times 10^{-6}\Delta\right))\right) \tag{11}$$

where N_b is the normality of the brine, given by

$$N_b = AS_{sw}\left(1.707 \times 10^{-2} + 1.205 \times 10^{-5}S_{sw} + 4.058 \times 10^{-9}S_{sw}^2\right) \tag{12}$$

and $A = 1.0$, corresponding to the assumption that the salt present was halite (NaCl). This assumption appears valid, as the observed soil water salinity concentrations were similar to the halite precipitation threshold and, in many areas, salt had precipitated at the surface. The static dielectric constant of brine ε_{b0} is given by

$$\varepsilon_{b0} = \varepsilon_{w0}\left(1.0 - 0.255N_b + 5.15 \times 10^{-2}N_b^2 - 6.89 \times 10^{-3}N_b^3\right). \tag{13}$$

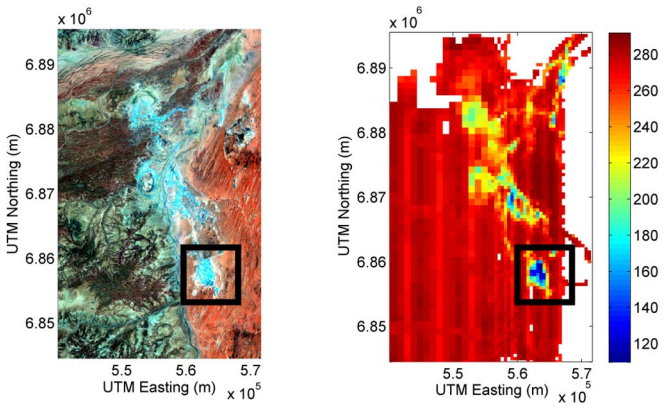

Fig. 2. Two images of the study area: (Left) Landsat false color and (right) airborne h-polarized L-band microwave brightness temperature at 38.5° incidence angle. The wet saline areas are clearly visible in the microwave image. Regions where brightness temperature is coldest coincide with (boxed area) saline areas. Coordinates are for Zone 53J UTM.

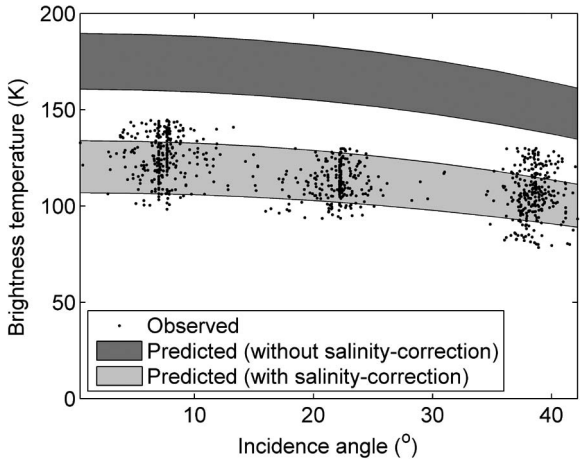

Fig. 3. Comparison of observed to predicted brightness temperatures over the groundwater discharge area.

The relaxation time for brine τ_b is given by

$$\tau_b = \tau_w \left(1.0 + 0.146 \times 10^{-2} T N_b - 4.89 \times 10^{-2} N_b - 2.97 \times 10^{-2} N_b^2 + 5.64 \times 10^{-3} N_b^3\right). \quad (14)$$

Salt was assumed to precipitate out of the soil water at 128 000 ppm, the value used in the only previous study [9]. While NaCl actually precipitates out of water at salinities more than double this concentration, the difference has a negligible effect on the results, and so, the lower precipitation threshold was retained, for consistency with the previous study.

IV. Results

A map of T_{bh} over the study region is shown in Fig. 2, together with a false-color Landsat image created using bands 5 (red), 2 (green), and 1 (blue), with histogram modifications made to highlight precipitated salt at the surface in blue. In this false-color image, the salt strongly absorbs short-wave infrared radiation in band 5, while reflecting it in bands 1 and 2. The lowest brightness temperatures observed coincide with several saline areas (the lowest temperatures are highlighted with black boxes). Striping in the T_{bh} map is due to varying incidence angles.

Simulations of L-band T_{bh} were conducted (Fig. 3) assuming wet or saturated conditions ($\theta = 0.30$ and 0.50 m^{3}m^{-3}, respectively) over a range of incidence angles, both with and without salinity corrections ($S_{SW} = 0$ ppm and $S_{SW} = 128\,000$ ppm, respectively), and compared to the lowest PLMR-footprint T_{bh} values observed over the wet patches of Nilpinna. Soil samples taken in saturated areas confirmed that saturated areas were at maximum salinity. The predicted ranges are based on typical soil conditions at the site: soil moisture between 0.30 and 0.50 m^{3}m^{-3}, gravimetric sand fraction of 67%, gravimetric clay fraction of 15%, bulk density of 1.3 g/cm^3, and soil temperature of 22.5 °C. Due to the three different incidence angles of PLMR, the observed brightness temperatures are clustered around the angles of 7°, 21.5°, and 38.5°. The simulated ranges of T_{bh} are distinctly separated by the soil water salinity, and the observed T_{bh}'s are scattered mostly within the saline range. It is clear that, without accounting for soil salinity, the forward model is unable to replicate the brightness temperatures observed. No observed brightness temperatures from the wet patches are in the expected range when salinity is neglected. Even assuming that the soil is saturated, the average difference between observed and predicted T_{bh}'s without correcting for salinity is 35 K. However, when soil salinity is included, 68% of the observed T_{bh} values fell within the expected bounds. These results are robust to reasonable changes in h: In particular, even decreasing h to 0.01 (an implausibly low value) results in only 3% of observations falling in the non-salinity-corrected range. The warm bias in predicted T_{bh} is consistent with the wet bias in retrieved soil moisture that occurs in the wettest patches, when salinity is not included in the brightness temperature model. For instance, the minimum observed gridded T_{bh} (500-m resolution) is 110 K (boxed in Fig. 2). Simulations of L-band T_{bh} were conducted over a range of θ (0–0.50 m^{3}m^{-3}) and S_{SW} values (0, 35 000, and 128 000 ppm) to identify whether such a low value could be attributed solely to high soil moisture (results not shown). The T_{bh} value could not be replicated using the forward model without a correction for salinity. Even with θ at saturation, the lowest simulated T_{bh}, without a salinity correction, was 21 K higher than the observed minimum. Note that this is lower than the 35-K average difference calculated earlier, as this difference is for a gridded average T_{bh} rather than a single PLMR footprint. If SMOS were to observe a pixel with $T_{bh} = 110$ K over an unvegetated area such as Nilpinna, it would infer $\theta = 1.0$ m^{3}m^{-3}, a value only physically possible for standing water, which was not present. In total, the observed T_{bh} was below the simulated minimum value for pure water in 0.6% of the study site (thirteen 500-m grid cells). However, as soil salinity is increased toward the threshold where precipitation occurs, the combination of high soil moisture and high salinity is able to produce the low T_{bh} values observed.

Of relevance to satellite missions like SMOS is understanding if this salinity effect is preserved at larger spatial scales. For a 51-km SMOS pixel over the site, the difference between average soil moisture retrievals without ($\bar{\theta}_{\mathrm{NSC}}$) and with ($\bar{\theta}_{\mathrm{SC}}$) a salinity correction across the study site (assuming a uniform

maximum salinity of 128 000 ppm) is 0.01 m^3m^{-3}. The soil moisture retrieval error due to salinity $\bar{\theta}_{\mathrm{NSC}} - \bar{\theta}_{\mathrm{SC}}$ is significant but less than the SMOS error budget (0.04 m^3m^{-3}), as the saline region at Nilpinna is relatively small. The error will be even greater for larger saline sites. It also interacts with the soil moisture of the saline sites: Salinity will have a much larger effect on retrievals at wet sites than at dry sites.

To quantify the scaling behavior of the salinity component of retrieval error with increasing saline proportion and soil moisture, a resampling method was employed (explained hereinafter), to increase the statistical power of the single image collected during the experiment. Averages of $\bar{\theta}_{\mathrm{SC}}$, $\bar{\theta}_{\mathrm{NSC}} - \bar{\theta}_{\mathrm{SC}}$, and saline proportion were calculated for moving windows within the study site, as in [21] for determining the effects of standing water on SMOS soil moisture retrievals. For each window, values of $\bar{\theta}_{\mathrm{SC}}$ and $\bar{\theta}_{\mathrm{NSC}} - \bar{\theta}_{\mathrm{SC}}$ were calculated in each 500-m pixel inside the window and averaged across the window. Window sizes ranged between 5% (1.6×2.6 km^2) and 50% (15.8×25.5 km^2) of the study site area, window overlap was 75% at most, and, for each window size, enough windows were used to fully cover the site. Since no direct observations of saline proportion exist, a 500-m pixel was assumed to be saline if the retrieved (salinity-corrected) soil moisture was greater than a threshold θ_{thresh}. The saline proportion for a window was calculated as the proportion of 500-m pixels classified as saline within that window. With groundwater as the only source of water at the study site, which is hypersaline in the upper soil layers, any areas wetter than the residual moisture content were classified as saline, i.e., θ_{thresh} was set to the residual moisture content (θ_r). Typical values of θ_r for the soil type observed at the site (sandy loam) range between 0.031 and 0.159 m^3m^{-3} [17]. For any given value of θ_{thresh}, the relationship between saline proportion and soil moisture retrieval error follows a similar linear trend, regardless of window size (not shown). This confirms that inferences can be made about the effect of salinity on larger windows, such as an SMOS footprint. The results are shown in Fig. 4, using $\theta_{\mathrm{thresh}} = 0.031$ m^3m^{-3}. Increasing soil moisture magnifies the salinity effect. Consequently, an SMOS pixel with as little as 25% saline area (13×13 km^2) and 0.04 m^3m^{-3} soil moisture would lead to retrieval errors greater than the entire SMOS error budget due to salinity alone. This is a conservative estimate of the total retrieval error over a saline site, as it does not include errors due to other factors, such as incomplete parameters, model structure, instrument error, etc. Note that the saline regions need not be clustered together; they could be distributed across the pixel, making identification and masking difficult. While this result is sensitive to the choice of θ_{thresh}, a conservative value has been used resulting in the largest required saline area to exceed the SMOS error budget. Using values at the higher end of the expected range results in the SMOS error budget being exceeded with less than 1% of the pixel saline (for average soil moisture of 0.04 m^3m^{-3}). Note that this analysis assumes that saline and moist areas coincide. Assessing the likely effects on SMOS pixels containing both pure and saline waters requires further field experiments.

This demonstrates the significant effect that fractional saline areas can have on large-scale soil moisture retrievals. Large-scale saline sites that cover multiple SMOS footprints, such as the Salar de Uyuni salt pan in Bolivia ($> 10\,000$ km^2), would result in erroneously wet-biased soil moisture retrievals, if they were not currently masked by SMOS. However, saline areas substantially smaller than a SMOS footprint may also cause serious errors. A small saline discharge area, such as the one at Nilpinna, will cause errors equivalent to 25% of the SMOS error budget; retrieval errors greater than the entire SMOS error budget will be caused by saline discharge areas less than a quarter of the size of an SMOS pixel. Large contiguous saline sites are rare and can be readily identified and masked. However, smaller more diffuse sites are more common and difficult to identify, meaning that they may easily go undetected, thus leading to significant errors. Consequently, it is important that soil moisture retrieval algorithms make a greater effort in accounting for saline areas, either through masking or improved retrieval algorithms.

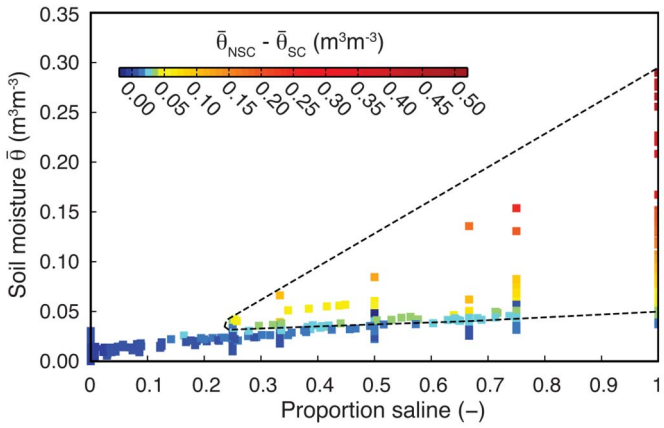

Fig. 4. Comparisons of retrieved soil moisture error due to salinity ($\bar{\theta}_{\mathrm{NSC}} - \bar{\theta}_{\mathrm{SC}}$) for windows of different sizes, with varying saline proportion and soil moisture ($\bar{\theta}$) as shown. Points represent a single window. The dashed-line polygon encloses all points representing windows with $\bar{\theta}_{\mathrm{NSC}} - \bar{\theta}_{\mathrm{SC}} \geq 0.04$ m^3m^{-3}; the color scale changes to yellow at $\bar{\theta}_{\mathrm{NSC}} - \bar{\theta}_{\mathrm{SC}} = 0.04$ m^3m^{-3}.

V. Conclusion

L-band soil moisture missions, such as SMOS, rely on corrections for factors such as surface roughness and vegetation to measure soil moisture. However, there may be other equally important factors that are not yet accounted for. This letter has investigated the effect of salinity on L-band microwave brightness temperature measurements at field scales. Airborne L-band brightness temperatures were measured in a saline environment near Nilpinna Station, South Australia. The observed brightness temperatures at PLMR-footprint resolution were substantially below simulated values when neglecting the salinity contribution. When averaged over 500-m pixels, 0.6% of the study site (13 pixels) showed brightness temperatures too low to be explained using the baseline algorithm for SMOS, even assuming soil saturation, without including a salinity correction. Importantly, it was shown that soil moisture retrieval errors of at least 0.04 m^3m^{-3} (i.e., the entire SMOS error budget) will occur in SMOS pixels with 0.04 m^3m^{-3} soil moisture and 25% saline coverage (possibly even much

less). This demonstrates the significance of fractional saline areas on soil moisture retrievals and the need for microwave satellite missions to consider the effects of salinity on soil moisture retrievals. Options to be considered include improving the retrieval algorithms to incorporate information on saline-affected areas or masking saline-affected pixels, rather than assuming that salinity will have a negligible effect on soil moisture retrievals.

ACKNOWLEDGMENT

The authors would like to thank all the participants in the Nilpinna field experiment (M. Allahmoradi, S. Hayes, J. Johansson, E. Kim, A. Marks, Y. Nan, S. Peischl, P. Richardson, and G. Tomlinson) and two anonymous reviewers, for substantially improving this paper.

REFERENCES

[1] E. G. Njoku and D. Entekhabi, "Passive microwave remote sensing of soil moisture," *J. Hydrol.*, vol. 184, pp. 101–129, 1996.

[2] D. Ryu, T. J. Jackson, R. Bindlish, and D. M. Le Vine, "L-band microwave observations over land surface using a two-dimensional synthetic aperture radiometer," *Geophys. Res. Lett.*, vol. 34, no. 14, p. L14 401, Jul. 2007.

[3] B. J. Choudhury, T. J. Schmugge, A. Chang, and R. W. Newton, "Effect of surface-roughness on the microwave emission from soils," *J. Geophys. Res.-Oceans Atmospheres*, vol. 84, no. C9, pp. 5699–5706, 1979.

[4] T. J. Jackson and T. J. Schmugge, "Vegetation effects on the microwave emission of soils," *Remote Sens. Environ.*, vol. 36, no. 3, pp. 203–212, Jun. 1991.

[5] K. R. Carver and T. F. Bush, *Airborne Multispectral Remote Sensing of Saline Seeps: The 1978 Harding Co., South Dakota Experiment*. Las Cruces, NM: New Mexico State Univ., 1979.

[6] K. Sreenivas, L. Venkataratnam, and P. V. N. Rao, "Dielectric properties of salt-affect soils," *Int. J. Remote Sens.*, vol. 16, no. 4, pp. 641–649, Mar. 1995.

[7] A. Stogryn, "Equations for calculating the dielectric constant of saline water," *IEEE Trans. Microw. Theory Tech.*, vol. MTT-19, no. 8, pp. 733–736, Aug. 1971.

[8] L. Chaturvedi, K. R. Carver, J. C. Harlan, G. D. Hancock, F. V. Small, and K. J. Dalstead, "Multispectral remote sensing of saline seeps," *IEEE Trans. Geosci. Remote Sens.*, vol. GRS-21, no. 3, pp. 239–251, Jul. 1983.

[9] T. Jackson and P. E. O'Neill, "Salinity effects on the microwave emission of soils," *IEEE Trans. Geosci. Remote Sens.*, vol. GRS-25, no. 2, pp. 214–220, Mar. 1987.

[10] F. Ghassemi, A. J. Jakeman, and H. A. Nix, *Salinisation of Land and Water Resources: Human Causes, Extent, Management and Case Studies*. Oxford, U.K.: CAB Int., 1995.

[11] S. K. McFeeters, "The use of normalized difference water index (NDWI) in the delineation of open water surfaces," *Int. J. Remote Sens.*, vol. 17, pp. 1425–1432, 1996.

[12] P. G. Slavich and G. H. Petterson, "Estimating the electrical-conductivity of saturated paste extracts from 1-5 soil, water suspensions and texture," *Aust. J. Soil Res.*, vol. 31, no. 1, pp. 73–81, 1993.

[13] "Diagnosis and improvement of saline and alkali soils," U.S. Dept. Agriculture, Washington, DC, 1954.

[14] T. Jackson, T. Schmugge, and J. R. Wang, "Passive microwave sensing of soil moisture under vegetation canopies," *Water Resour. Res.*, vol. 18, no. 4, pp. 1137–1142, 1982.

[15] W. T. Crow, S. T. K. Chan, D. Entekhabi, P. R. Houser, A. Y. Hsu, T. J. Jackson, E. G. Njoku, P. E. O'Neill, J. Shi, and X. Zhan, "An observing system simulation experiment for hydros radiometer-only soil moisture products," *IEEE Trans. Geosci. Remote Sens.*, vol. 43, no. 6, pp. 1289–1303, Jun. 2005.

[16] M. J. Escorihuela, Y. Kerr, P. De Rosnay, J.-P. Wigneron, J.-C. Calvet, and F. Lemaitre, "A simple model of the bare soil microwave emission at L-band," *IEEE Trans. Geosci. Remote Sens.*, vol. 45, no. 7, pp. 1978–1987, Jul. 2007.

[17] W. J. Rawls, L. R. Ahuja, D. L. Brakensiek, and A. Shirmohammadi, "Infiltration and soil water movement," in *Handbook of Hydrology*, D. Maidment, Ed. New York: McGraw-Hill, 1993.

[18] M. C. Dobson, F. T. Ulaby, M. T. Hallikainen, and M. A. El-Rayes, "Microwave dielectric behavior of wet soils 2. Dielectric mixing models," *IEEE Trans. Geosci. Remote Sens.*, vol. GRS-23, no. 1, pp. 35–46, Jan. 1985.

[19] F. T. Ulaby, R. K. Moore, and A. K. Fung, *Microwave Remote Sensing (Active and Passive): From Theory to Applications*. Norwood, MA: Artech House, 1986.

[20] L. A. Klein and C. T. Swift, "Improved model for dielectric-constant of sea-water at microwave frequencies," *IEEE Trans. Antennas Propag.*, vol. AP-25, no. 1, pp. 104–111, Jan. 1977.

[21] J. P. Walker, O. Merlin, and R. Panciera, *National Airborne Field Experiment 2006 (NAFE'06): Experiment Plan*. Melbourne, Australia: Univ. Melbourne, 2006.